Effect of permeability on steady flow in a dendrite layer

D. N. Riahi
Department of Theoretical and Applied Mechanics
216 Talbot Laboratory, 104 South Wright Street
University of Illinois at Urbana-Champaign
Urbana, Illinois 61801 U. S. A.

ABSTRACT

We consider the problem of nonlinear steady convective flow in a horizontal dendrite layer during alloy solidification. We analyze the effect of permeability of the layer on the stationary modes of convection in the form of two-dimensional rolls and three-dimensional patterns. Under a near-eutectic approximation and the limit of large far-field temperature, we determine the two- and three-dimensional solutions to the weakly nonlinear problem by using a perturbation technique, and the stability of these solutions are investigated with respect to arbitrary three-dimensional disturbances. An inverse form of the permeability function introduces two non-negative non-dimensional parameters K_1 and K_2 that are significant in the present problem. The results of the analyses in particular range of values of the magnitude $|\varepsilon|$ of the amplitude of convection indicate, in particular, that the effects of K_1 and K_2 on the flow pattern are destabilizing and stabilizing, respectively, and different types of flow pattern can be stable for particular values of these parameters. For sufficiently small and non-zero values of $|\varepsilon|$ and K_1, the steady flow pattern in the form of subcritical hexagons can stable. For $|\varepsilon|$ beyond some value and depending on the values of the parameters of the problem, supercritical rolls, squares or rectangles can be stable. For K_1=0.0, the only stable flow pattern is that due to steady rolls.

1. INTRODUCTION

The present study considers the problem of finite-amplitude steady convection in a horizontal dendrite layer, sometimes called mushy layer, during alloy solidification. The investigation is based on the mushy-layer model developed by Amberg and Homsy (1993) and Anderson and Worster (1995) where a near –eutectic approximation was employed in the limit of large far-field temperature. The model allows examination of the dynamics of the dendrite layer in the form of small deviation from the classical system of convection in a horizontal porous layer of constant permeability. Such single-layer model focuses on the mushy-layer mode of convective flow, which is one of the two modes of convection discovered by Worster (1992) in a two-layer system. Amberg and Homsy (1993) made a number of simplifying assumptions including those stated above and the ones that the thickness of the dendrite layer is small and such layer is isolated from the overlying liquid layer. In addition, the authors assumed that the value of the Stefan number S_t, representing the latent heat release, due to solidification, is of order one and the amplitude ε of convection is of the same order as the thickness δ of the dendrite layer. The form of the finite-amplitude steady convection studied by Amberg

and Homsy (1993) was that due to either two-dimensional rolls or hexagons. They found that two-dimensional rolls were supercritical for sufficiently small values of the parameter K_1 and subcritical if K_1 was sufficiently large, and steady hexagons were found to be transcritical.

Anderson and Worster (1995) extended the weakly nonlinear analysis of Amberg and Homsy (1993) to the limit of large S_t and the case $\varepsilon<<\delta<<1$. They applied a double-series expansion in powers of ε and δ for the rescaled variables and the Rayleigh number R. They focused on the steady modes of convection for K_1 of order δ and calculated the finite amplitude steady solutions in the form of two-dimensional rolls and hexagons and analyzed the stability using their derived evolution equation for the small amplitude coefficients of the steady rolls and hexagons. They found that hexagons can be stable for sufficiently small $|\varepsilon|$, while steady rolls can be stable for $|\varepsilon|$ beyond some value.

In the present investigation, we consider the steady problem by following Anderson and Worster (1995) in assuming a much wider range of values for the amplitude of convection, but considering finite-amplitude analyses for squares and rectangular cells in addition to rolls and hexagons, investigating the effects of the parameters K_1 and K_2 on such flow patterns and carrying out stability analysis of the finite-amplitude steady solutions. We found a number of interesting results. In particular, we found that supercritical squares and supercritical rectangles can be the stable and preferred flow patterns for particular range of values of the parameters and ε where rolls and hexagons are unstable. However, subcritical rectangles and subcritical squares, which can exist in particular range of values of the parameters, are found to be unstable.

2. GOVERNING SYSTEM

We consider a binary alloy melt that is cooled from below and is solidified at a constant speed V_0. Following Amberg and Homsy (1993) and Anderson and Worster (1995), we consider a dendrite layer of thickness d adjacent and above the solidification front to be physically isolated from the overlying liquid and the underlying solid zones. The overlying liquid is assumed to have a composition $C_0>C_e$ and temperature $T_\infty >T_L(C_0)$ far above the mushy layer, where C_e is the eutectic composition, $T_L(\tilde{C})$ is the liquidus temperature of the alloy and $\tilde{C}$ is the composition. It is then assumed that the horizontal dendrite layer is bounded from above and below by rigid and isothermal boundaries. We consider the solidifying system in a moving frame of reference $o\tilde{x}\tilde{y}\tilde{z}$, whose origin lies on the solidification front, translating at the speed V_0 with the solidification front in the positive $\tilde{z}$-direction.

It should be noted that no double-diffusive effect is present in the above described one-layer dendrite-zone model since such a dendrite layer is assumed to be in local thermodynamic equilibrium and, thus,

$$\tilde{T}=T_L(C_0)+\Gamma(\tilde{C}-C_0),$$

where $\tilde{T}$ is the temperature and Γ is the slope of the liquidus (Anderson and Worster 1995), which is assumed to be constant. The dendrite layer is treated appropriately as a porous layer (Fowler1985; Worster1992), where the solid dendrites and the liquid coexist, and Darcy's law is adopted.

Next, we consider the equations for momentum, continuity, heat and solute for the flow of melt in the mushy layer in the already described moving frame. These equations

are non-dimensionalized by using V_0, k/V_0, k/V_0^2, $\beta\Delta C\ \rho gk/V_0$, ΔC and ΔT as scales for velocity, length, time, pressure, solute and temperature, respectively. Here k is the thermal diffusivity, ρ is a reference (constant) density, $\beta = \beta^* - \Gamma\alpha^*$, where α^* and β^* are the expansion coefficients for the heat and solute, respectively, $\Delta C = C_0 - C_e$, $\Delta T = T_L(C_0) - T_e$ and T_e is the eutectic temperature. The non-dimensional form of the equations for momentum, continuity, temperature and solute concentration in the mushy layer are

$$K(\tilde{\phi})\tilde{\mathbf{u}} = -\nabla\tilde{P} - \tilde{R}\,\tilde{\theta}\mathbf{z}, \tag{1a}$$

$$\nabla.\tilde{\mathbf{u}} = 0, \tag{1b}$$

$$(\partial/\partial\,\tilde{t} - \partial/\partial\tilde{z})(\tilde{\theta} - S_t\tilde{\phi}) + \tilde{\mathbf{u}}.\nabla\tilde{\theta} = \nabla^2\tilde{\theta}, \tag{1c}$$

$$(\partial/\partial\,\tilde{t} - \partial/\partial\,\tilde{z}\,)[(1-\tilde{\phi})\theta + C_r\tilde{\phi}] + \tilde{\mathbf{u}}\,.\nabla\tilde{\theta} = 0, \tag{1d}$$

where $\tilde{\mathbf{u}} = \tilde{u}\mathbf{x} + \tilde{v}\mathbf{y} + \tilde{w}\mathbf{z}$ is the volume flux vector per unit area, which is also known as Darcy velocity vector (Nield1998), $\tilde{u}$ and $\tilde{v}$ are the horizontal components of $\tilde{\mathbf{u}}$ along $\tilde{x}$- and $\tilde{y}$-directions, respectively, $\mathbf{x}$ and $\mathbf{y}$ are unit vectors along the positive $\tilde{x}$- and $\tilde{y}$-directions, $\tilde{w}$ is the vertical component of $\tilde{\mathbf{u}}$ along $\tilde{z}$-direction, $\mathbf{z}$ is a unit vector along the positive $\tilde{z}$-direction, $\tilde{P}$ is the modified pressure, $\tilde{\theta}$ is the non-dimensional composition, or equivalently temperature (Worster1992), $\tilde{\theta} = [\tilde{T} - T_L(C_0)]/\Delta T = (\tilde{C} - C_0)/\Delta C$, $\tilde{t}$ is the time variable, $\tilde{\phi}$ is the local solid fraction, $\tilde{R} = \beta\Delta C g\,\Pi(0)/(V_0\nu)$ is the Rayleigh number, $\Pi(0)$ is reference value at $\tilde{\phi}=0$ of the permeability $\Pi(\tilde{\phi}\,)$ of the porous medium, which is assumed to be finite (Worster1992), ν is the kinematic viscosity, g is acceleration due to gravity, $K(\tilde{\phi}) \equiv \Pi(0)/\Pi(\tilde{\phi})$, $S_t = L/(C_L\Delta T)$ is the Stefan number, C_L is the specific heat per unit volume, L is the latent heat of solidification per unit volume, $C_r = (C_s - C_0)/\Delta C$ is a concentration ratio and C_s is the composition of the solid-phase forming the dendrites. The equation (1d) is based on the limit of sufficiently large value of the Lewis number k/k_s (Worster1992; Anderson and Worster1995), where k_s is the solute diffusivity.

The governing equations (1a)-(1d) are subject to the following boundary conditions (Amberg and Homsy1993):

$$\tilde{\theta} + 1 = \tilde{w} = 0 \quad \text{at } \tilde{z} = 0, \tag{2a}$$

$$\tilde{\theta} = \tilde{w} = \tilde{\phi} = 0 \quad \text{at } \tilde{z} = \delta, \tag{2b}$$

where $\delta = dV_0/k$ is a growth Peclet number representing the dimensionless depth of the layer.

Following Amberg and Homsy and Anderson and Worster (1995) in reducing the model asymptotically, we assume the following rescaling in the limit of sufficiently small δ:

$$C_r = C/\delta,\ S = S_t/\delta,\ \varepsilon << \delta << 1, \tag{3a}$$

$$(\tilde{x}, \tilde{y}, \tilde{z}) = (x, y, z)\delta\ ,\ \tilde{t} = \delta^2\, t,\ R^2 = \delta\tilde{R}, \tag{3b}$$

$$\tilde{\theta}= \theta_B(z)+\varepsilon\theta(x, y, z, t), \tag{3c}$$

$$\tilde{\phi}= \phi_B(z)+\varepsilon\phi(x, y, z, t), \tag{3d}$$

$$\tilde{\mathbf{u}}=0+ (\varepsilon R/\delta)\mathbf{u}(x, y, z, t), \tag{3e}$$

$$\tilde{P}=RP_B(z)+R\varepsilon P(x, y, z,t), \tag{3f}$$

where C and S are order one quantities as $\delta\rightarrow 0$, and the quantities with subscript 'B' are the basic flow variables for the motionless state and are assumed to be a function of z only. The small deviation of each dependent variable from its basic quantity is measured by a perturbation amplitude ε and can vary with respect to spatial and time variables as shown in (3c)-(3f).

As discussed in Anderson and Worster (1995), the assumption of thin mushy layer ($\delta <<1$) is associated with large non-dimensional far-field temperature $\theta_\infty=[T_\infty - T_L(C_0)]/ \Delta T>>1$, which can occur when the initial $\tilde{C}$ is close to C_e . The assumption of order one quantity C corresponds to the near-eutectic approximation (Fowler1985), which allows one to describe the mushy layer as a porous layer of constant permeability to the leading order.

The rescaling (3a)-(3f) are then used in (1a)-(1d) and (2a)-(2b). This system of equations and boundary conditions admits a motionless basic state, which is steady and horizontally uniform. The basic state solution is given below in terms of the asymptotic expansions for $\delta<<1$:

$$\theta_B=(z-1)+ \delta(z-z^2)G/2+..., \; G\equiv 1+S/C, \tag{4a}$$

$$\phi_B= \delta(1-z)/C+ \delta^2[-(1-z)^2/C^2 +(z^2-z)G/(2C)]+..., \tag{4b}$$

$$P_B=P_0+R[(z-z^2/2)+\delta(z^2/2-z^3/3)G/2+...], \tag{4c}$$

where P_0 is a constant. Since $\tilde{\phi}$ is expected to be small, according to (4b), the following expansion for $K(\tilde{\phi})$ will be implemented later in the governing system:

$$K(\tilde{\phi})=1+K_1\tilde{\phi} +K_2 \tilde{\phi}^{\,2}+..., \tag{5}$$

where K_1 and K_2 are constants (Amberg and Homsy1993).

For the analysis to be presented in the next section, it is convenient to use the general representation

$$\mathbf{u}= \boldsymbol{\Omega}V+\mathbf{E}\psi, \tag{6a}$$

$$\boldsymbol{\Omega}\equiv\nabla\times\nabla\times\mathbf{z}, \;\; \mathbf{E}\equiv\nabla\times\mathbf{z}, \tag{6b}$$

for the divergent-free vector field **u** (Chandrasekhar1961). Here V and ψ are the poloidal and toroidal functions for **u**, respectively. By taking the vertical component of the curl of (1a) it can be shown that the toroidal part $\mathbf{E}\psi$ of **u** must vanish. Taking the vertical

components of the double curl of (1a) and using (1b) in (1)-(2), we find the following system which will be analyzed in the next section

$$\nabla^2 [K(\phi_B+\varepsilon\phi)\Delta_2 V]+(\partial/\partial z)[\mathbf{\Omega}V.\nabla K(\phi_B+\varepsilon\phi)]-R\Delta_2\theta =0, \quad (7a)$$

$$(\partial/\partial t-\delta\partial/\partial z)(-\theta+S\phi/\delta)+R(d\theta_B/dz)\Delta_2 V+\nabla^2\theta=\varepsilon R(\mathbf{\Omega}V).\nabla\theta, \quad (7b)$$

$$(\partial/\partial t-\partial/\partial z)[(-1+\phi_B)\theta+\theta_B\phi+\varepsilon\phi\theta-C\phi/\delta]+ R(d\theta_B/dz)\Delta_2 V =\varepsilon R(\mathbf{\Omega}V).\nabla\theta, \quad (7c)$$

$$\theta=V=0 \quad \text{at } z=0, \quad (7d)$$

$$\theta=V=\phi=0 \quad \text{at } z=1, \quad (7e)$$

where

$$\Delta_2 \equiv \partial^2/\partial x^2+\partial^2/\partial y^2.$$

3. ANALYSIS

In this section we seek steady-state solutions of the nonlinear system (7a)-(7f) by applying a weakly nonlinear analysis, based on a double series expansions in powers of two small parameters for the perturbation quantities, of the type carried out by Busse (1967) and Busse and Riahi (1980). Here the small parameters are δ and ε, which satisfy the condition given in (3a). Following Anderson and Worster (1995), we first make a formal asymptotic expansion in ε and then at each order in ε make a formal asymptotic expansion in δ. The appropriate expansions are for the dependent variables of the perturbation system and for R. These expansions are given below

$$(V, \psi, \theta, \phi, R)=[(V_{00}+\delta V_{01}+...), (\psi_{00}+\delta\psi_{01}+...), (\theta_{00}+\delta\theta_{01}+...), (\phi_{00}+\delta\phi_{01}+...), (R_{00}+\delta R_{01}$$

$$+...)]+\varepsilon[(V_{10}+\delta V_{11}+...), (\psi_{10}+\delta\psi_{11}+...), (\theta_{10}+\delta\theta_{11}+...), (\phi_{10}+\delta\phi_{11}+...), (R_{10}+\delta R_{11}+...)]$$

$$+\varepsilon^2[(V_{20}+\delta V_{21}+...), (\psi_{20}+\delta\psi_{21}+...), (\theta_{20}+\delta\theta_{21}+...), (\phi_{20}+\delta\phi_{21}+...), (R_{20}+\delta R_{21}+...)]+... \quad (8)$$

3.1. Linear prooblem

Upon inserting (8) into (7a)-(7f) and disregarding the nonlinear terms, we find the linear problem. At order $\varepsilon^0\delta^0$ the system (7a)-(7f) yield the following results:

$$V_{00}=[(\pi^2+a^2)/(R_{00}a^2G)]\sin(\pi z)\sum_n{}^{N}{}_{=-N} A_n W_n, \quad (9a)$$

$$\theta_{00}= -\sin(\pi z)\sum_n{}^{N}{}_{=-N} A_n W_n, \quad (9b)$$

$$\phi_{00}=[-(\pi^2+a^2)/(GC\pi)][1+\cos(\pi z)]\sum_n{}^{N}{}_{=-N} A_n W_n, \quad (9c)$$

$$R_{00}{}^2=(\pi^2+a^2)^2/(Ga^2), \quad (9d)$$

where

$$W_n=\exp(i\mathbf{a}_n.\mathbf{r}). \tag{9e}$$

Here i is the pure imaginary number ($i^2 = -1$), subscript 'n' takes only non-zero integer values from –N to N, N is a positive integer representing the number of distinct modes, **r** is the position vector, and the horizontal wave number vectors $\mathbf{a}_n$ satisfy the properties

$$\mathbf{a}_n.\mathbf{z} =0, |\mathbf{a}_n| =a, \mathbf{a}_{-n} = -\mathbf{a}_n. \tag{10}$$

The coefficients A_n are constants and satisfy the conditions

$$\sum_{n=-N}^{N} A_n A_n^{*}=1, \quad A_n^{*}=A_{-n}, \tag{11}$$

where the asterisk indicates the complex conjugate. Minimizing the expression for R_{00} given in (9d), with respect to the wave number a, we find

$$R_{00c}=2\pi/\sqrt{G}, \tag{12a}$$

$$a_c= \pi. \tag{12b}$$

Here R_{00c} is the minimum value of R_{00} achieved at $a=a_c$. In all the analyses and solutions to follow, hereafter, we shall set $R_{00}=R_{00c}$ and $a=a_c$, unless indicated otherwise.

Considering the governing system (7a)-(7e) in the order $\varepsilon^0\delta^1$, multiplying the equation (7a) by aV_{00} and (7b) by θ_{00}, adding these two later equations, averaging over the fluid layer and making use of (7d)-(7e), we find the condition for the existence of the solutions V_{01} and θ_{01}. This condition yield

$$R_{01}=[\pi K_1/(2C\sqrt{G})]+2\pi G_t\sqrt{G}(1/4+2/\pi^2),\ G \equiv(G-1)/(CG^2). \tag{13}$$

Hence, the critical Rayleigh number R_c for the linear system can be written as

$$R_c=R_{00c}+\delta R_{01c}+ O(\delta^2). \tag{14}$$

The solutions in this order can be written in the form

$$(V_{01}, \theta_{01}, \phi_{01})=[V_{01}^{*}(z), \theta_{01}^{*}(z), \phi_{01}^{*}(z)]\sum_{n=-N}^{N} A_nW_n, \tag{15}$$

where the expressions for the coefficients V_{01}^{*}, θ_{01}^{*} and ϕ_{01}^{*}, which are functions of z and the non-dimensional parameters of the problem, are given by (A1a)-(A1h) in appendix.

3.2. Nonlinear problem

Next, we analyze the nonlinear problem for the steady convection. The solvability conditions for the nonlinear systems require the following special solutions V_{00n} and θ_{00n} of the linear system:

$$(V_{00n}, \theta_{00n})=[(\pi^2+a^2)/(\sqrt{G}R_{00}a^2), -1] \sin(\pi z)A_n W_n. \quad (16)$$

It turns out that there is no need to consider special linear solution for ϕ since the governing nonlinear systems are usually reduced to a form where only (16) will be needed to form the corresponding solvability conditions. Consider the system (7a)-(7e) in order ε. Multiplying the equation (7a) by $-V_{00n}$, (7b) by θ_{00n}, adding, averaging over the fluid layer and applying the boundary conditions (7d)-(7e), we find

$$R_{10}|A_n|^2= - 3K_1\pi^2/(CG^{1.5}) \sum_{l,p} (1+\Phi_{lp})A_n A_l A_p <W_n W_l W_p >, \quad (17a)$$

where

$$\Phi_{lp}=\mathbf{a}_l.\mathbf{a}_p /a^2, \quad (17b)$$

and an angular bracket indicates the average over the layer. The right-hand-side in (17a) for R_{10} indicates that R_{10} =0, unless

$$\mathbf{a}_n +\mathbf{a}_l +\mathbf{a}_p =0 \quad (18)$$

for at least some l and p. The condition (18) can be satisfied in the cases where convection is in the form of hexagons (Busse1967), while (18) can not be satisfied for convection in the form of two-dimensional rolls, squares or rectangles. The solutions in this order can be written in the form

$$(V_{10}, \theta_{10}, \phi_{10})=[V_{10}^*(z), \theta_{10}^*(z), \phi_{10}^*(z)]\sum_{n=-N}^{N} A_n W_n +\sum_{l,p} [V_{10}\hat{}(z,\Phi_{lp}), \theta_{10}\hat{}(z,\Phi_{lp}),$$

$$\phi_{10}\hat{}(z,\Phi_{lp})]\sum_{l,p} A_l A_p W_l W_p, \quad (19)$$

where the expressions for V_{10}^*, θ_{10}^*, ϕ_{10}^*, $V_{10}\hat{}$, $\theta_{10}\hat{}$ and $\phi_{10}\hat{}$ are lengthy and will not be given in this paper.

We now consider the system (7a)-(7f) in order ε^2. Multiplying the equation (7a) by $-V_{00n}$, (7b) by θ_{00n}, adding, averaging over the fluid layer and applying the boundary conditions (7d)-(7e), we find

$$R_{20}|A_n|^2= \sum_{l,m,p} F_{20}(\Phi_{lp}, \Phi_{ml}, \Phi_{mp})A_n A_l A_m A_p <W_n W_l W_m W_p>+ \sum_{l,p} H_{20}(\Phi_{lp})A_n A_l A_p$$

$$<W_n W_l W_p>+G_{20}|A_n|^2, \quad (n=-N, ..., -1, 1, ..., N), \quad (20)$$

where the summations in (20) for l, m and p run from –N to N, and the expressions for F_{20}, H_{20} and G_{20} are quite lengthy and will not be given in this paper.

The system (20) contains integral expressions of the form $<W_n W_l W_p>$, which differ from zero only if (18) is satisfied, and integral expressions of the form $<W_n W_l W_m W_p>$, which differ from zero only if

$$\mathbf{a}_n +\mathbf{a}_l +\mathbf{a}_m +\mathbf{a}_p=0. \quad (21)$$

The system (21), together with (11), (17a) and (20), can be used to study the steady solutions in the form of two-dimensional rolls and three-dimensional cells. We shall restrict our attention to the simplest types of solutions, which include those observed in the applications. These solutions are called regular or semi-regular solutions (Busse1967). In the case of a regular solution all angles between two neighboring **a**-vectors are equal and (11) yield

$$|A_1|^2=...=|A_N|^2=1/(2N). \tag{22}$$

In the more general semi-regular solution, where (22) still holds, the scalar products between any of the **a**-vectors and its two neighboring **a**-vectors assume the constant values α_1 and α_2. An example of a semi-regular solution is that due to rectangular cells (N=2), where $\alpha_1 = - \alpha_2$. Regular solutions can follow from the semi-regular ones for the special case $\alpha_1= \alpha_2$. Simple forms of regular solutions correspond to the cases of two-dimensional rolls (N=1), square cells (N=2) and hexagons (N=3).

Thus, using (11), (18) and (21)-(22) in (17a), (20) and (21), we find

$$R_{10} =[-3K_1\pi^2/(CG^{1.5}\sqrt{6})]\mathbf{S}, \tag{23a}$$

$$R_{20}=\sum_{m=-N}^{N} T_{nm}|A_m|^2+(2/\sqrt{6})H_{20}(\Phi_{lp}=0.5)\mathbf{S}+ G_{20}, \quad (n=-N, ..., -1, 1, ..., N), \tag{23b}$$

where

$$\mathbf{S}=1 \text{ for hexagons and } 0 \text{ for non-hexagons}, \tag{23c}$$

$$T_{nm}=F_{-n,n,-n}\,\delta_{nm}+(F_{n,-n,-n}+F_{-n,-n,n})\delta_{n,-m}+(F_{-m,m-n}+F_{-n,m,-m}+F_{m,-n,-m})(1-\delta_{nm})(1-\delta_{n,-m}),\ F_{l,m,p}$$

$$\equiv F_{20}(\Phi_{lp}, \Phi_{ml}, \Phi_{mp}), \tag{23d}$$

$$\delta_{nm}=1 \text{ for } n=m \text{ and } 0 \text{ for } n \neq m. \tag{23e}$$

Here by the term 'non-hexagons' in (23c) it is meant solution whose wave number vectors do not contain a sub-set of such vectors, which can satisfy a condition of the type (18).

The simplest types of solutions, which turn out to be preferred under certain conditions in the present study, are described briefly as follows. For steady two-dimensional rolls, N=1, $A_n=1/\sqrt{2}$ and **S**=0 in (23). For rectangular pattern convection, N=2, $A_n=1/2$, $\gamma\neq90°$ and **S**=0 in (23). Here γ is the angle ($\gamma\leq90°$) between two adjacent wave number vectors of any cell. For square pattern convection, N=2, $A_n=1/2$, $\gamma=90°$ and **S**=0 in (23). For hexagonal convection, N=3, $A_n =1/\sqrt{6}$ and **S**=1 in (23). As will be referred to later in section 4, the sign of the vertical motion at the cells' centers for hexagons, which is determined by the sign of ε, is inferred from the condition

$$\varepsilon R_{10}<0 \tag{24}$$

for the preferred subcritical hexagons. As can be seen from (23a), the value of R_{10} in the present problem is negative, and, thus, the sign of the vertical motion at the cells' centers for the subcritical hexagons is positive, and such hexagons are referred to as up-hexagons (Busse1967). By analogy, the sign of the vertical motion at the cells' centers for the supercritical hexagons is negative in the present problem, and such hexagons are referred to as down-hexagons.

3.3. Stability problem

The analysis of the nonlinear steady convection presented in the previous sub-section has shown that an infinite manifold of solutions could exist even though this manifold represents only an infinitesimal fraction of the manifold of the solutions (9a)-(9d) of the linear problem. To distinguish the physically realizable solution among all the possible steady solutions, the stability of V, θ, ϕ with respect to arbitrary three-dimensional disturbances V_d, θ_d, ϕ_d need to be investigated. The time-dependent disturbances can be assumed in the form

$$(V_d, \theta_d, \phi_d)=[V'(x, y, z), \theta'(x, y, z), \phi'(x, y, z)]\exp(\sigma t), \tag{25}$$

where σ is the growth rate of the disturbances. When the governing equations and the boundary conditions of the form (7a)-(7f) for the finite-amplitude steady flow are subtracted from the corresponding equations and boundary conditions for the total dependent variables for the steady flow and the disturbance quantities and the resulting system is linearized with respect to the disturbance quantities, we obtain the stability system, which is given by (A2a)-(A2e) in the appendix.

When the expansion (8) is used in (A2a)-(A2e), it becomes evident that the stability system can be solved by a similar expansion

$$\begin{aligned}(V', \theta', \phi',\sigma)=&[(V'_{00}+\delta V'_{01}+...), (\theta'_{00}+\delta\theta'_{01}+...), (\phi'_{00}+\delta\phi'_{01}+...), (\sigma_{00}+\delta\sigma_{01}+...)]+ \varepsilon[(V'_{10}\\ &+\delta V'_{11}+...), (\theta'_{10}+\delta\theta'_{11}+...), (\phi_{1(-1)} /\delta+\phi'_{10}+\delta\phi'_{11}+...), (\sigma_{10}+\delta\sigma_{11}+...)]+\varepsilon^2[(V_{2(-1)}/\delta+V'_{20}+\\ &\delta V'_{21} +...), (\theta_{2(-1)}/\delta+\theta'_{20}+\delta\theta'_{21}+...), (\phi_{2(-1)}/\delta+\phi'_{20}+\delta\phi'_{21}+...), (\sigma_{20}+\delta\sigma_{21}+...)]+... ,\end{aligned} \tag{26}$$

where the expansions for ϕ' and all the disturbance variables are singular at order ε and ε^2, respectively, as $\delta\to 0$, but, it turns out, that such $O(1/\delta)$ terms are needed in the stability analysis since it is found that the $O(\varepsilon)$ and $O(\varepsilon^2)$ of the stability problem are forced by terms of order $1/\delta$ in the equations for the disturbances.

For the present stability analysis we restrict ourselves to those disturbances whose dependent variables have wave number vectors $\mathbf{a}'_n$, which all have the same wave number $|\mathbf{a}'_n|= a'=a_c$. Then the most critical disturbances, which have the maximum growth rate, are found to be characterized by $\sigma_0 =0$, where

$$\sigma_0=\sigma_{00}+\delta\sigma_{01}+...$$

The linear solutions for the dependent variables of the disturbances at order δ^0 are found to be of the form (9a)-(9d), provided A_n, W_n and N are replaced by arbitrary constants $\tilde{A}_n$, $\tilde{W}_n = \exp(i\mathbf{a}'_n.\mathbf{r})$ and ∞, respectively.

In analogy to the solvability conditions for the steady motion presented in the previous sub-section, the solvability conditions for the disturbance systems in the order ε (n>1) require us to define particular solutions of the linear system for the disturbance system. These solutions designated by $\tilde{V}_{00n}$ and $\tilde{\theta}_{00n}$ have the same form as (15), provided A_n and W_n are replaced, respectively, by $\tilde{A}_n$ and $\tilde{W}_n$. The solvability condition for the disturbance system in the order ε is derived similar to the corresponding one for the steady flow system. We first derived the disturbance system at order ε from (A2a)-(A2e). Next, we multiplied the equation (A2a) by $-\tilde{V}_{00n}$, (A2b) by $\tilde{\theta}_{00n}$, added, averaged over the fluid layer and applied the boundary conditions (A2d)-(A2e). We then found the expression for σ_{10}. Similarly, we applied the solvability conditions in the order ε^2 to determine σ_{20}. Since σ_{10} or σ_{20} may not in general be zero for a particular solution, we define

$$\sigma^* = \varepsilon\sigma_{10} + \varepsilon^2\sigma_{20} \tag{27a}$$

as the leading order growth rate and combine the solvability conditions in the orders ε and ε^2 to obtain the following system for σ^*:

$$(-\sigma^* M + R^*)|\tilde{A}_n|^2 = \sum_{l,p} [\varepsilon L_{10}(\Phi_{lp}, \Psi_{lp}) + \varepsilon^2 L_{20}(\Phi_{lp}, \Psi_{lp})](\tilde{A}_n \tilde{A}_l A_p \langle \tilde{W}_n \tilde{W}_l W_p \rangle + \tilde{A}_n A_l \tilde{A}_p \langle \tilde{W}_n W_l \tilde{W}_p \rangle) + \sum_{l,m,p} \varepsilon^2 [F_{20}(\Phi_{lp}, \Phi_{ml}, \Phi_{mp}) + \tilde{F}_{20}(\Phi_{lp})(\Psi_{ml} + \Psi_{mp})](\tilde{A}_n \tilde{A}_l A_m A_p \langle \tilde{W}_n \tilde{W}_l W_m W_p \rangle + \tilde{A}_n A_l \tilde{A}_m A_p \langle \tilde{W}_n W_l \tilde{W}_m W_p \rangle + \tilde{A}_n A_l A_m \tilde{A}_p \langle \tilde{W}_n W_l W_m \tilde{W}_p \rangle), \tag{27b}$$

where

$$R^* = \varepsilon R_{10} + \varepsilon^2 (R_{20} - G_{20}), \tag{27c}$$

$$\Psi_{lp} = [(\mathbf{a}_l \times \mathbf{a}_p).\mathbf{z}]/a^2, \tag{27d}$$

$$M = R_{00}/[2(\pi^2 + a^2)], \tag{27e}$$

and the expressions for $\tilde{F}_{20}$, L_{10} and L_{20} are too lengthy and will not be given in this paper. The growth rates σ^* of the disturbances acting on the finite-amplitude steady motion can then be determined from (27) following the method of approach due to Busse (1967), which is now a standard stability procedure, for cases where the wave number vectors of the disturbances either coincide with those of the steady motion or not.

4. DISCUSSION AND RESULTS

4.1. Linear problem

The linear system and its eigenvalue problem, which led to the results (9)-(15), are, in general, functions of the parameters G and G_t. These two parameters represent S and C in a composite manner. The present results are provided for given values of G and

G_t. It should also be noted that for the experimental results due to Tait et al. (1992), the values of G and G_t are evaluated to be about $G \approx 1.25$ and $G_t \approx 0.008$. The results presented in the present paper are mostly for the range of values $0.833 \le S \le 6.667$ and $3.333 \le C \le 26.667$, which correspond to $G=1.25$ and $0.006 \le G_t \le 0.048$. Here and thereafter value of $\delta=0.2$ is chosen to evaluate R_c and other quantities whose values may depend on δ. The linear results indicate that a_c is a constant independent of the parameters, while R_c depends on G, G_t and K_1. The value of R_c decreases with increasing G and increases weakly with increasing either G_t or K_1. Thus, R_c is destabilizing with respect to G and stabilizing with respect to either G_t or K_1. The stabilizing effect on the linear system when K_1 increases, is consistent with the physical role played by K_1 since the permeability of the dendrite layer decreases with increasing K_1. Since S represents a measure of the latent heat relative to the heat content and C represents the difference between the characteristic composition of the solid and liquid phases and the compositional variation of the liquid, the linear system is destabilized as S increases for a given C, or as C decreases for a given S. Hence, the linear system is destabilized as G increases. Since G_t increases with decreasing C, for a given G, S has to decrease by the same rate as C in order to maintain the value of G. Thus, our linear result about stabilizing effect of G_t implies that S is more effective than C in stabilizing the flow as G_t increases.

Due to degeneracy of the linear system, the above described linear results are applicable to both two- and three-dimensional convection cases whose nonlinear results are presented and discussed in the next sub-section.

4.2. Nonlinear problem

Important quantities due to the nonlinear effects are the coefficients R_{10} and R_{20}, which are calculated in the present study. As can be seen from the expansions (8), these coefficients represent leading contributions to the change in R required to obtain finite amplitude ε for a nonlinear solution. In terms of these coefficients the amplitude of convection is of order

$$|\varepsilon| = \{|R_{10}| \pm [R_{10}^2 + 4R_{20}(R-R_c)]^{0.5}\}/(2R_{20}). \tag{28}$$

As can be seen from (28), there are two expressions for $|\varepsilon|$ corresponding to plus and minus signs in (28), where the expression with plus sign corresponds to the case where R_{20} is positive, while the expression with negative sign corresponds to the case where R_{20} is negative. It should also be noted that in the case of non-zero R_{10}, which can correspond to the cases where convection is in the form of hexagons, then the expression (28) for $|\varepsilon|$ is provided only for the preferred subcritical convection state where $R<R_c$. In this case the amplitude of convection is largest if the magnitude of R_{10} is largest. For $R_{10}=0$, which can correspond to the cases of two-dimensional rolls, rectangles and square pattern convection, then the sign of R_{20} determines whether the steady solution exists for values of R above or below R_c. For $R_{10}=0$ and supercritical convection, where $R>R_c$, the amplitude of convection is largest, provided the value of R_{20} is smallest among all the solutions to the nonlinear problem. In the present problem the coefficients R_{10} and R_{20} are due to the nonlinear convective terms in the temperature equation and the nonlinear interactions between the flow velocity and the non-uniform and nonlinear permeability associated with the perturbation to the basic state solid fraction.

Hexagonal convection

The coefficient R_{10}, given by (23a), for the hexagonal convection was computed for various values of G, G_t and K_1. As (23a) indicates, this coefficient is independent of K_2 and its dependence on C is converted into dependence on G and G_t. It can be seen that R_{10} is negative, and, thus, the steady hexagonal convection can be supercritical for $\varepsilon < 0$ and subcritical for $\varepsilon > 0$. Thus, for supercritical case, down-hexagons are predicted, while up-hexagons are predicted for the subcritical case.

Some typical results about the effects of G_t and K_1 are presented in Figure 1 for R_{10} versus G_t for G=1.25 and for several values of K_1. It is seen from this figure that R_{10} decreases with increasing either G_t or K_1, and the rate of decrease of R_{10} with respect to either G_t or K_1 increases with increasing either K_1 or G_t. Hence, the nonlinear results to the order ε indicate stabilizing and destabilizing effects of these parameters on the supercritical and subcritical hexagons, respectively.

The coefficient R_{20}, given by (23b), for the hexagonal convection (N=3, $A_n=1/\sqrt{6}$), designated here by $R_{20}^{(h)}$, was computed for various values of G, G_t, K_1 and K_2. It was found that $R_{20}^{(h)}$ is positive for sufficiently small K_1. For $K_1=0.0$, it is independent of G_t, but it increases with K_2. For $K_1 \neq 0$, $R_{20}^{(h)}$ increases with K_2, decreases with increasing either K_1 or G_t and becomes negative for sufficiently large K_1. Some typical results about the variation of $R_{20}^{(h)}$ with respect to G_t for $K_1=0.1$, 1.0 and 3.0 are presented in Figure 2 for $K_2=0.0$. It is seen from this figure that the rate of decrease of $R_{20}^{(h)}$ with respect to K_1 or G_t increases with K_1. Hence, although K_2 has stabilizing effect, both K_1 and G_t have destabilizing effect as far as the value of $R_{20}^{(h)}$ is concerned. Although variations of R_{10} with respect to different parameters provide information about various destabilizing and stabilizing features for the hexagonal convection, as was presented and discussed in the last two paragraphs, it should be noted that information about R_{20} for hexagons is useful in the sense that since R_{20} is the leading second-order coefficient in the expansion for R in powers of ε, $R_{20}^{(h)}$ plays useful roles in calculating the solute flux and the order of magnitude of ε in (28) and in cases where R_{10} becomes negligible or for the stability consideration of hexagons that will be discussed in the next sub-section.

Square pattern convection

We now present and discuss the result for another three-dimensional case of convection whose form is that of square cells, which, as is discussed later, could become prefer in the present problem for K_1 in particular range of values.

As was explained in the previous section, R_{10} is zero for the case where convection is in the form of square cells, and, thus, we present and discuss the results for the coefficient R_{20}, given by (23b), for the square cells (N=2, $A_n=1/2$), which is designated here by $R_{20}^{(s)}$. This coefficient was computed for various values of G_t, K_1 and K_2. It was found that, depending on the value of K_1, $R_{20}^{(s)}$ can be positive or negative and, thus, both supercritical and subcritical squares can be possible. Also, $R_{20}^{(s)} < R_{20}^{(h)}$. For $K_1=0.0$, $R_{20}^{(s)}$ is positive and independent of G_t, but it increases with K_2, which is consistent with the stabilizing effect of decreasing the permeability. For $K_1 \neq 0$, $R_{20}^{(s)}$ increases with K_2, and it decreases with increasing either K_1 or G_t. Some typical results about the variation of $R_{20}^{(s)}$ with respect to G_t for $K_1=0.1$, 1.0 and 3.0 are presented in Figure 3 for $K_2=0.0$. As in the case of $R_{20}^{(h)}$, it is seen from this figure that the rate of decrease of $R_{20}^{(s)}$ with respect to either K_1 or G_t increases with K_1, and $R_{20}^{(s)}$ decreases rapidly with G_t for sufficiently high value of K_1. Hence, again destabilizing effects of K_1

and G_t are apparent. The square pattern convection can be supercritical only for sufficiently small value of K_1 and subcritical for sufficiently large value of K_1.

Rectangular pattern convection

The simplest semi-regular solutions in the form of different types of rectangular patterns are found to become preferred in the present problem for K_1 above some value K_{c1}. Similar to the case of squares, R_{10} is zero for rectangles. For K_1 just above K_{c1}, which appears to decrease with increasing G_t, rectangles with angle γ about 90° (squares) are supercritical and their R_{20} value, which is designated for general rectangle by $R_{20}^{(re)}$, is smaller than the corresponding ones for other rectangles with different angles γ and rolls. As is discussed later, there is an interesting pattern transitional phenomenon in the sense that γ decreases continuously with increasing K_1 until γ reaches a value very close to 0° and the rolls become the preferred flow structure over the rectangles. Each one of such rectangular solutions is found to have the smallest value of $R_{20}^{(re)}$ over some interval in K_1 in the domain $0°<\gamma<90°$.

The coefficient $R_{20}^{(re)}$ was computed for various values of G_t, K_1, γ and K_2. It was found that $R_{20}^{(re)}$ is positive for K_1 below some critical value K_{c2} and negative for K_1 above K_{c2}. The value of K_{c2} depends in general on G_t and γ ($0°<\gamma<90°$), and it decreases with increasing G and γ. Thus, both supercritical and subcritical rectangles can exist in particular range of values for K_1. As in the case of squares, $R_{20}^{(re)}<R_{20}^{(h)}$. The qualitative results about variations of $R_{20}^{(re)}$ with respect to K_2 are similar to those for squares. Some typical results about the variations of $R_{20}^{(re)}$ with respect to G_t and K_1 are shown in Figure 4 for G=1.25, K_2=0.0 and γ=50°. It can be seen from this figure that the effect of increasing K_1 and G_t are destabilizing, and the rate of decrease of $R_{20}^{(re)}$ with respect to either K_1 and G_t increases with K_1.

Two-dimensional rolls

As was explained in the previous section, R_{10} is zero for two-dimensional rolls. Thus, the important coefficient for rolls (N=1, $A_n=1/\sqrt{2}$) is R_{20} given in (23b), which is designated here by $R_{20}^{(r)}$. This coefficient was computed for various values of G_t, K_1 and K_2. It was found that for sufficiently small K_1, $R_{20}^{(r)}$ is positive and rolls are supercritical, while rolls are subcritical for K_1 beyond some value, which depends on G_t. Also, $R_{20}^{(r)}<R_{20}^{(re)}$. For K_1=0.0, $R_{20}^{(r)}$ is independent of G_t , but it increases with K_2. For $K_1\neq 0$, $R_{20}^{(r)}$ increases with K_2 and it decreases with increasing either K_1 or G_t. Some calculated results about the variation of $R_{20}^{(r)}$ with respect to G_t for different values of K_1 (Figure 5) indicated that the rate of decrease of $R_{20}^{(r)}$ with respect to either K_1 or G_t increases with K_1. Hence, destabilizing effects of G_t and K_1 and stabilizing effect of K_2 on rolls follow.

Figure 6 presents some typical results about comparison between the variation of the coefficient R_{20} with respect to G_t for rolls, squares, rectangles for γ=40° and hexagons. These results are for G=1.25, K_1=3.0 and K_2 =6.0. These values of K_1 and K_2 were chosen based on the permeability model used by Worster (1992) where

$$K(\tilde{\phi})=1/(1-\tilde{\phi}) =1+3.0\tilde{\phi} +6.0\tilde{\phi}^2 +... \qquad (29)$$

Comparing (29) to (5) implies K_1=3.0 and K_2=6.0. The model used by Worster (1992) is consistent with the experimental evidence about the permeability variation with respect to the porosity subjected to the Amberg and Homsy (1993) model for the single dendrite layer.

It can be seen from the figure 6 that G_t has destabilizing effect on all such patterns , supercritical rectangles can be realized at a lower value of the Rayleigh number than other supercritical flow cases, and squares are subcritical throughout the considered range for G_t. In addition, supercritical hexagons are generally realized at a value of R larger than those due to rolls, rectangles and squares, and R_{20} for all such flow cases is negative for sufficiently large values of G_t.

4.2. Stability of steady finite-amplitude solutions

Following standard stability procedure (Busse1967), the system (27b) for the growth rate σ^* of the disturbances acting on the finite-amplitude steady solutions has been simplified, and the expression for σ^* has been computed for different integers N and various values of the quantities Φ_{nm} ($|\Phi_{nm}|\leq 1$) and Ψ_{nm} ($|\Psi_{nm}|\leq 1$). In all the cases that have been investigated only steady supercritical solutions in the form of rolls, rectangles and squares, and subcritical steady solutions in the form of up-hexagons with $R_{20}^{(h)}>0$ are found to be possibly stable in particular range of values for the non-dimensional parameters and for ε. The results are briefly as follows. Supercritical rolls are stable only if

$$|\varepsilon|\geq\varepsilon_1,\ \varepsilon_1=\sqrt{3}|R_1|/R_{20}^{(r)},\ 0<R_{20}^{(r)}\leq R_{20}^{(s)},\ 0<R_{20}^{(r)}\leq R_{20}^{(re)}. \tag{30a}$$

Supercritical squares are stable only if

$$|\varepsilon|\geq\varepsilon_2,\ \varepsilon_2=\sqrt{3}|R_1|/[\sqrt{2}(R_{20}^{(r)}-R_{20}^{(s)})],\ R_{20}^{(r)}>R_{20}^{(s)}>0,\ R_{20}^{(re)}\geq R_{20}^{(s)}>0. \tag{30b}$$

Supercritical rectangles are stable only if

$$|\varepsilon|\geq\varepsilon_3,\ \varepsilon_3=\sqrt{3}|R_1|/[\sqrt{2}(R_{20}^{(r)}-R_{20}^{(re)})],\ R_{20}^{(r)}>R_{20}^{(re)}>0,\ R_{20}^{(s)}\geq R_{20}^{(re)}>0. \tag{30c}$$

Subcritical up-hexagons are stable only if

$$\varepsilon_4\leq|\varepsilon|\leq\varepsilon_5,\ \varepsilon_4=|R_1|/R_{20}^{(h)},\ \varepsilon_5=6|R_1|/(R_{20}^{(h)}-R_{20}^{(r)}). \tag{30c}$$

Figure 7 provides a qualitative bifurcation diagram for the case (29) representing the amplitude ε versus R for those solutions, which can possibly be stable in particular range of ε according to the results provided in (30). Solid lines correspond to linearly stable branches while dotted lines correspond to linearly unstable branches. Note that no representation is given in this diagram of any three-dimensional solution that is always unstable. This bifurcation diagram provides different cases for possibly stable solutions. For sufficiently small G_t in the range $0<G_t\leq G_{t1}$, square-branch ($\gamma=90°$) bifurcates supercritically and is initially unstable to a subcritically bifurcating up-hexagonal branch. For $G_{t1}<G_t<G_{t2}$, rectangular-branch ($0°<\gamma<90°$) bifurcates supercritically and is initially unstable to a subcritically bifurcating up-hexagonal branch. Here the critical values G_{t1} and G_{t2} for G_t correspond to the bifurcation points for square- and roll-branches, respectively. For $G_{t1}\leq G_t\leq G_{t2}$ and as G increases just above its lower-bound value, the supercritical square-branch is replaced by a supercritical rectangular-branch for γ just below 90° and γ decreases continuously with increasing G_t until roll-branch ($\gamma\rightarrow 0°$), which replaces the rectangular branch, bifurcates supercritically at $G_t=G_{t2}$ and is initially

unstable to subcritically bifurcating up-hexagonal branch. For K_1=0.0, supercritical rolls represent the only stable flow pattern.

5. CONCLUSION AND SOME REMARKS

We investigated the problem of nonlinear steady convection in a dendrite layer during alloy solidification. We analyzed the two- and three-dimensional steady modes of convection in the dendrite layer using the model due to Amberg and Homsy (1993). We performed a weakly nonlinear analysis to determine the steady solutions admitted by the nonlinear problem and carried out stability analysis to determine the solutions that can be stable with respect to arbitrary three-dimensional disturbances in different ranges of the values of the parameters and ε. We found that, depending on the range of values of the parameters and ε, two-dimensional rolls and three-dimensional solutions in the form of squares, rectangles and up-hexagons can be possibly stable. We found that two-dimensional rolls are supercritical and stable only if $|\varepsilon|$ is equal to or above some value ε_1 and G_t is within some range of values $G_{t2} \le G_t \le G_{t3}$. Three-dimensional squares (rectangles) are stable only if they are supercritical, $|\varepsilon|$ is equal to or above some value ε_2 (ε_3) and G_t lies in the range $0<G_t \le G_{t1}$ ($G_{t1}<G_t<G_{t2}$). Subcritical squares and subcritical rectangles also can exist but they are unstable. Subcritical up-hexagons are stable only if $R_{20}^{(h)}>0$ and ε lies in the range $\varepsilon_4 \le |\varepsilon| \le \varepsilon_5$. Supercritical down-hexagons can exist but they are unstable. There are certain overlap regions in ε where more than one solution can be stable and, thus, hysteretic effect can be non-zero in such overlap regions. The stability of supercritical rectangles and squares uncovered in the present study was found to be entirely due to the realistic permeability dependence on the porosity.

The conclusion presented in the previous paragraph and the results shown in the figures 6-7 indicate that no steady solution can be stable for $G_t>G_{t3}$, which raises the question as to what solutions can be possibly stable in the range of the parameter values where no steady solution is stable. Although the investigation of the problem for answering such question is beyond the scope of the present study, it should be noted that non-steady solutions of the present model, such as oscillatory modes of convection in a mushy layer (Riahi2002), which has been studied only for very small values of $K_1<<1$, may need to be determined and analyzed for order one values of K_1 compatible with the expansion (29) to see if can provide an answer to the above question or other possibilities may need to be explored. Some preliminary investigation of the oscillatory flow cases for order one values of K_1 indicated that the perturbation approach predicts too high values of the coefficient R_{20}, which violates the validity of the expansion of the type (8), and, thus, numerical approach need to be used to carry out such investigation.

Finally, in regard to the available experimental result, the one due to Tait et al. (1992) predicted down-hexagons in the flow of 28% ammonium chloride solution solidified from its base in a square tank. Such result has not yet been predicted by any theoretical studies of the mushy-layer model that have been done in the last decade or so. However, it should be noted that such experimental study was conducted at the Rayleigh number about one order of magnitude higher than that at the onset of convection, while the present results are strictly valid close to the onset of convection. Unfortunately, no experimental results near the onset of convection in a mushy layer are available yet to confirm the present theoretical results.

APPENDIX

The expressions for the coefficients $V_{01}^{*}(z)$, $\theta_{01}^{*}(z)$ and $\phi_{01}^{*}(z)$ are

$$(V_{01}^{*}, \theta_{01}^{*})=(b_1, c_1)\, z \sin(\pi z)+(b_2, c_2)z \cos(\pi z)+(b_3, c_3)z^2 \cos(\pi z)+(b_4, c_4)\sinh(rz)+(b_5, c_5)\cosh(rz)+(b_6, c_6)\cos(\pi z)+(b_7, c_7)\sin(\pi z), \quad \text{(A1a)}$$

$$\phi_{01}^{*}=b_0+(R_{00}a^2/C)\{b_1[-(z/\pi)\cos(\pi z)+(1/\pi^2)\sin(\pi z)]+b_2[(z/\pi)\sin(\pi z)+(1/\pi^2)\cos(\pi z)]+b_3[(z^2/\pi)\sin(\pi z)+(2/\pi^2)z\cos(\pi z)-(2/\pi^3)\sin(\pi z)]+(b_4/r)\cosh(rz)+(b_5/r)\sinh(rz)+(b_6/\pi)\sin(\pi z)-(b_7/\pi)\cos(\pi z)\}-[(2R_{01}+R_{00})a^2(\pi^2+a^2)/(2C\pi R_{00}a^2)+1/(\pi C^2)](\pi^2+a^2)\cos(\pi z)+(1/C)[1-(\pi^2+a^2)/(C\pi^2)]\sin(\pi z)+(-1+1/C)(\pi^2+a^2)[1/(\pi C)][-z\cos(\pi z)+(1/\pi)\sin(\pi z)]-[(\pi^2+a^2)/(\pi C^2)]z, \quad \text{(A1b)}$$

where

$$b_2=(\pi^2+a^2)[2R_{01}+R_{00}/2]/d_1,\ d_1\equiv 4\pi(\pi^2+a^2),\ r=\{(2a^2+d_0^{0.5})/2\}^{0.5},\ d_0\equiv 4a^2R_{00}^2, \quad \text{(A1c)}$$

$$b_3=-(\pi^2+a^2)R_{00}/(2d_1),\ b_1=\{-R_{00}-b_3(4a^2+12\pi^2)\}/d_1,\ b_4=(\pi^2 d_2+d_3)/[(\pi^2+r^2)\sinh(r)], \quad \text{(A1d)}$$

$$d_2\equiv b_3+[1+\cosh(r)](2\pi b_1+2b_3)/(\pi^2+r^2),\ b_7=1, \quad \text{(A1e)}$$

$$d_3\equiv 2\pi b_1+(2-\pi^2)b_3+[\pi^2-r^2\cosh(r)](-2\pi b_1-2b_3)/(\pi^2+r^2),\ b_5=(-2\pi b_1-2b_3)/(\pi^2+r^2)=-b_6, \quad \text{(A1f)}$$

$$c_1=[-\pi(\pi b_1+4b_3)-a^2b_1]/R_{00},\ (c_2, c_3)=-(b_2, b_3)(\pi^2+a^2)/R_{00},\ (c_4, c_5)=(b_4, b_5)(r^2-a^2)/R_{00}, \quad \text{(A1g)}$$

$$c_6=(-\pi^2b_6+2\pi b_1+2b_3-a^2b_6)/R_{00},\ c_7=(-\pi^2-2\pi b_2-a^2+R_{01})/R_{00}. \quad \text{(A1h)}$$

The stability system for the present problem is given below

$$\nabla^2\{\varepsilon[K_1\phi'+K_2(2\phi_B+2\varepsilon\phi)\phi']\Delta_2 V+K(\phi_B+\varepsilon\phi)\Delta_2 V'\}+(\partial/\partial z)\{\varepsilon\mathbf{\Omega}V.\nabla[K_1\phi'+K_2(2\phi_B+2\varepsilon\phi)\phi']+\mathbf{\Omega}V'\cdot\nabla K(\phi_B+\varepsilon\phi)\}-R\Delta_2\theta'=0, \quad \text{(A2a)}$$

$$(\partial/\partial t-\delta\partial/\partial z)(-\theta'+S\phi'/\delta)+R(d\theta_B/dz)\Delta_2 V'+\nabla^2\theta'=\varepsilon R[\mathbf{\Omega}V.\nabla\theta'+\mathbf{\Omega}V'.\nabla\theta], \quad \text{(A2b)}$$

$$(\partial/\partial t-\delta\partial/\partial z)[(-1+\phi_B)\theta'+\theta_B\phi'+\varepsilon\phi\theta'+\varepsilon\phi'\theta-C\phi'/\delta]+R(d\theta_B/dz)\Delta_2 V'=R\varepsilon[\mathbf{\Omega}V.\nabla\theta'+(\mathbf{\Omega}V').\nabla\theta], \quad \text{(A2c)}$$

$$V'=\theta'=0 \text{ at } z=0, \quad \text{(A2d)}$$

$$V'=\theta'=\phi' \text{ at } z=1. \quad \text{(A2e)}$$

REFERENCES

AMBERG, G. AND HOMSY, G. M. 1993 Nonlinear analysis of buoyant convection in binary solidification with application to channel formation. J. Fluid Mech. **252**, 79-98.

ANDERSON, D. M. AND WORSTER, M. G. 1995 Weakly nonlinear analysis of convection in mushy layers during the solidification of binary alloys. J. Fluid Mech. **302**, 307-331.

Busse, F. H. 1967 The stability of finite-amplitude convection and its relation to an extremum principal. J. Fluid Mech. **30**, 625-649

Busse, F. H. AND RIAHI, D. N. 1980 Nonlinear convection in a layer with nearly insulating boundaries. J. Fluid Mech. **96**, 243-256.

CHANDRASEKHAR, S. 1961 Hydrodynamic and Hydromagnetic Stability, Oxford: Clarendon Press.

FOWLER, A. C. 1985 The formation of freckles in binary alloys. IMA J. Appl. Maths **35**, 159-174

NIELD, D. A. 1998 Instability and turbulence in convective flows in porous media. In Nonlinear Instability, Chaos and Turbulence, edited by L. Debnath and D. N. Riahi, WIT Press, UK, **1**, 225-276.

RIAHI, D. N. 2002 On nonlinear convection in mushy layers Part 1.Oscillatory modes of convection. J. Fluid Mech. **467**, 331-359.

TAIT, S., JAHRLING, K. AND JAUPART, C. 1992 The planform of compositional convection and chimney formation in a mushy layer. Nature **359**, 406-408.

WORSTER, M. G. 1992 Instabilities of the liquid and mushy regions during solidification of alloys. J. Fluid Mech. **237**, 649-669.

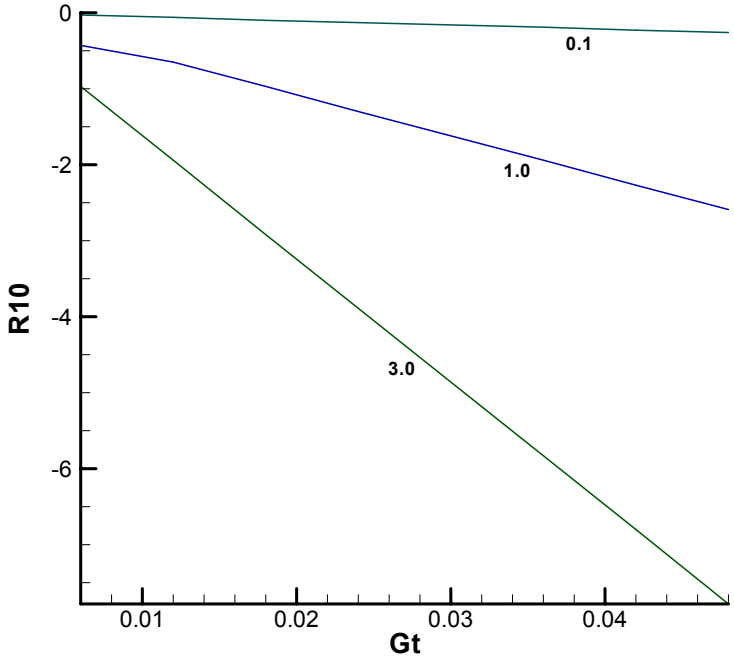

Figure 1. R_{10} versus G_t for hexagons. Here G=1.25, and graphs are for K_1=0.1, 1.0 and 3.0.

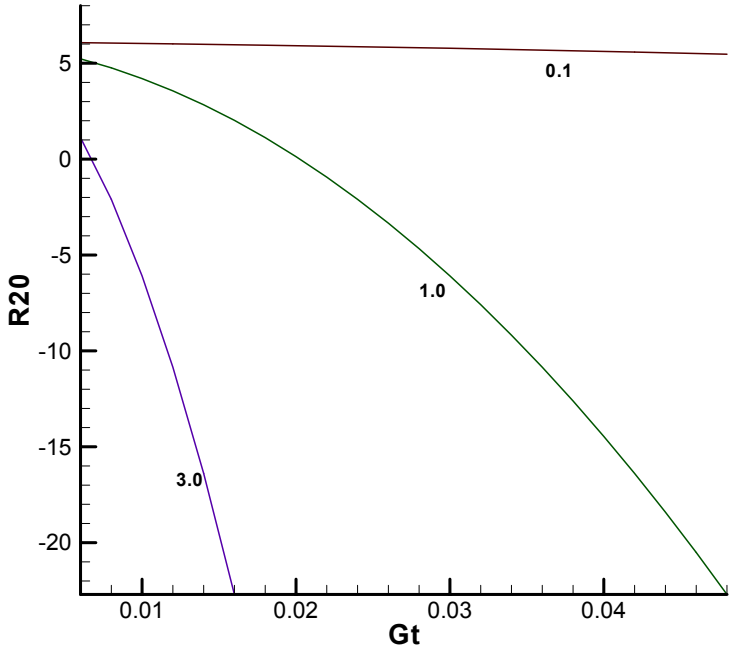

Figure 2. R_{20} versus G_t for hexagons. Here G=1.25 and K_2=0.0, and graphs are for K_1 = 0.1, 1.0 and 3.0.

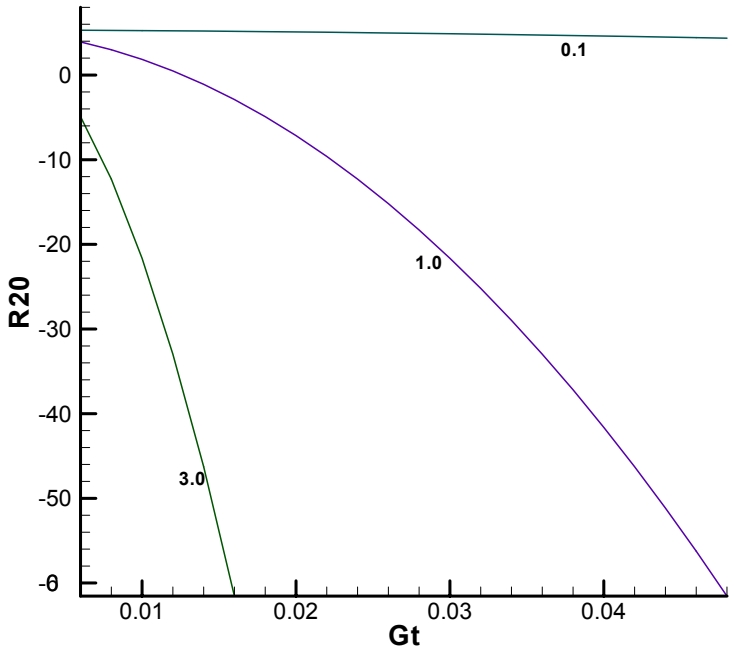

Figure 3. R_{20} versus G_t for squares. Here G=1.25 and K_2=0.0, and graphs are for K_1 = 0.1, 1.0 and 3.0.

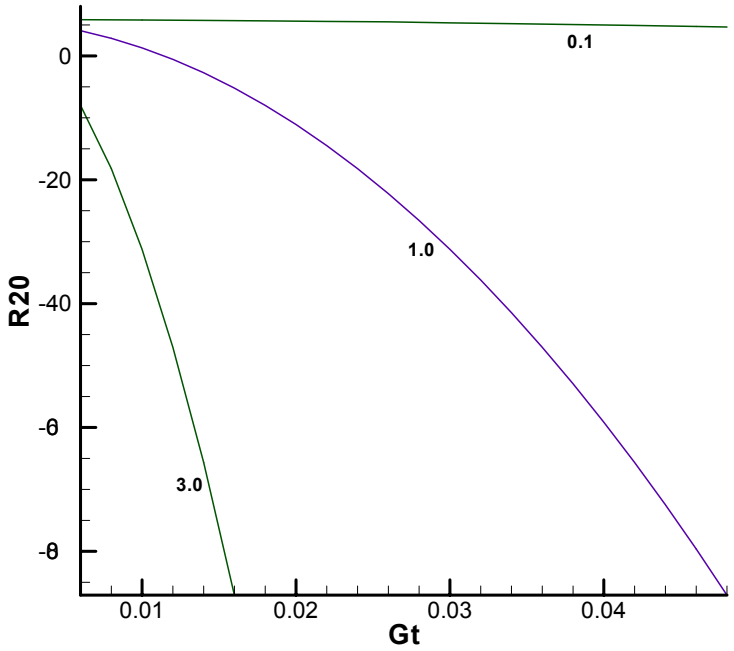

Figure 4.R_{20} versus G_t for rectangles. Here G=1.25, γ=50° and K_2=0.0. The graphs are for K_1=0.1, 1.0 and 3.0.

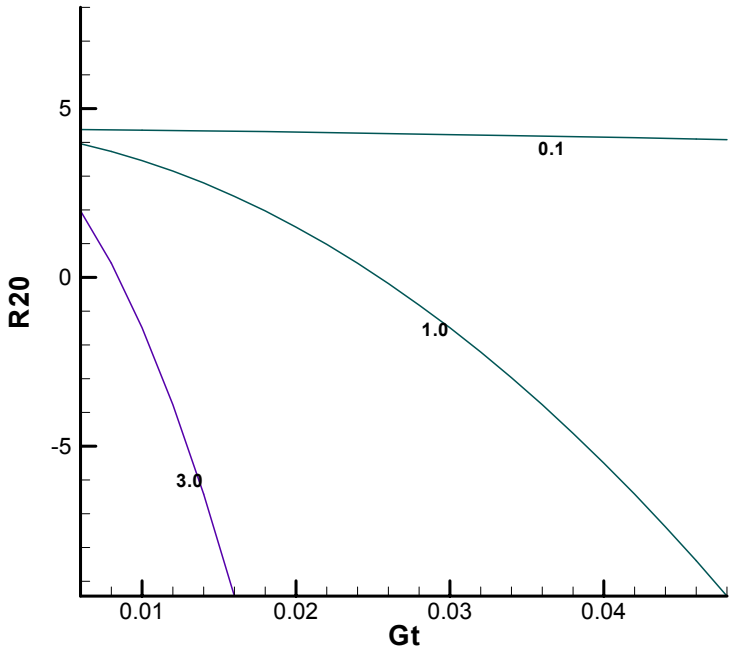

Figure 5. R_{20} versus G_t for rolls. Here G=1.25 and K_2=0.0, and graphs are for K_1=0.1, 1.0 and 3.0.

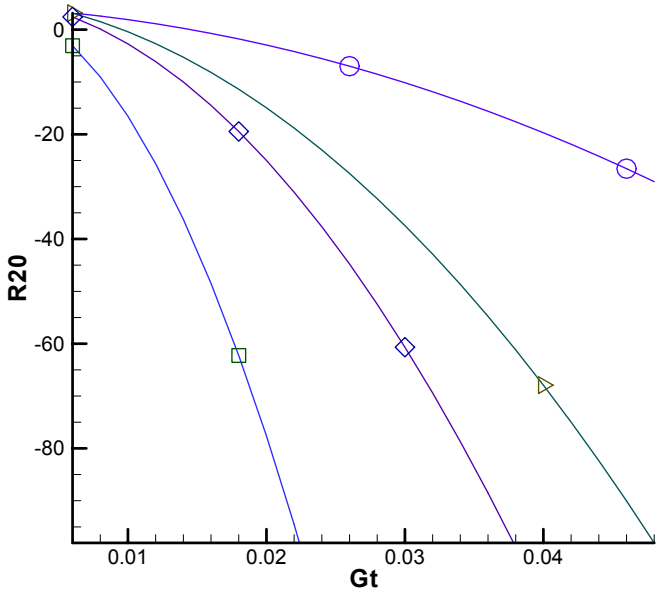

Figure 6. R_{20} versus G_t for rolls, squares, rectangles and hexagons. Here K_1=3.0, G= 1.25 and K_2 =0.0. The graphs labeled by the symbols of circle, square, diamond and triangle present, respectively, R_{20} for rolls, squares, rectangles with γ=40° and hexagons.

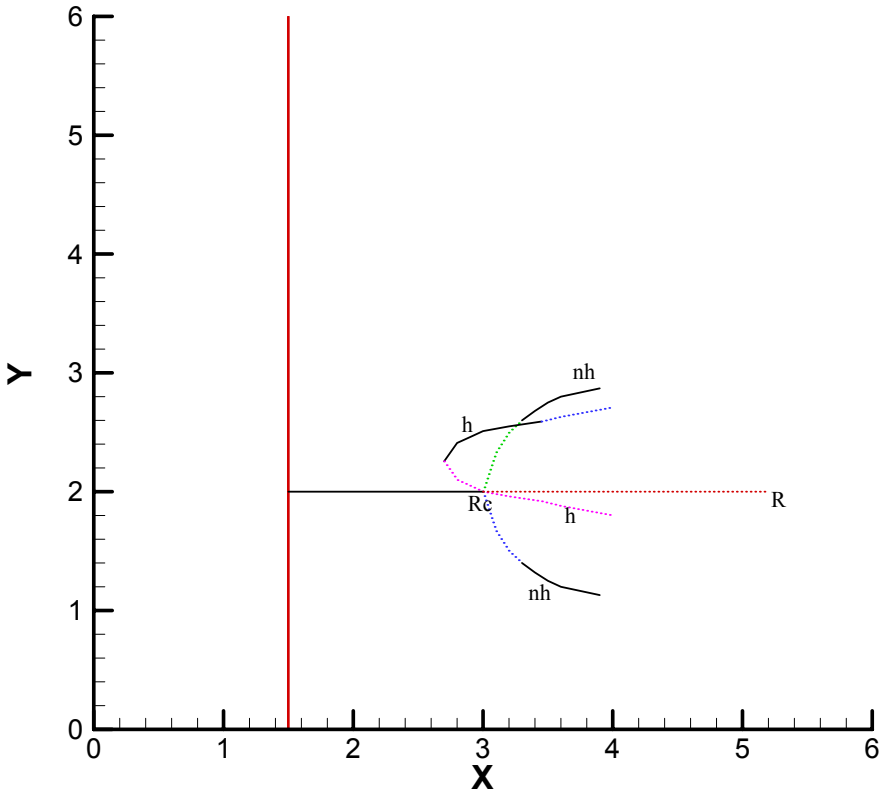

Figure 7. Bifurcation diagram in (R, ε)-plane. Here solid and dotted lines present, respectively, stable and unstable branches. The lines labeled by h and nh present, respectively, hexagons and non-hexagonal cases.

List of Recent TAM Reports

No.	Authors	Title	Date
966	Bagchi, P., and S. Balachandar	Linearly varying ambient flow past a sphere at finite Reynolds number: Part 2—Equation of motion—*Journal of Fluid Mechanics* **481**, 105–148 (2003) (with change in title)	Feb. 2001
967	Cermelli, P., and E. Fried	The evolution equation for a disclination in a nematic fluid—*Proceedings of the Royal Society A* **458**, 1–20 (2002)	Apr. 2001
968	Riahi, D. N.	Effects of rotation on convection in a porous layer during alloy solidification—Chapter 12 in *Transport Phenomena in Porous Media* (D. B. Ingham and I. Pop, eds.), 316–340 (2002)	Apr. 2001
969	Damljanovic, V., and R. L. Weaver	Elastic waves in cylindrical waveguides of arbitrary cross section—*Journal of Sound and Vibration* (submitted)	May 2001
970	Gioia, G., and A. M. Cuitiño	Two-phase densification of cohesive granular aggregates—*Physical Review Letters* **88**, 204302 (2002) (in extended form and with added co-authors S. Zheng and T. Uribe)	May 2001
971	Subramanian, S. J., and P. Sofronis	Calculation of a constitutive potential for isostatic powder compaction—*International Journal of Mechanical Sciences* (submitted)	June 2001
972	Sofronis, P., and I. M. Robertson	Atomistic scale experimental observations and micromechanical/continuum models for the effect of hydrogen on the mechanical behavior of metals—*Philosophical Magazine* (submitted)	June 2001
973	Pushkin, D. O., and H. Aref	Self-similarity theory of stationary coagulation—*Physics of Fluids* **14**, 694–703 (2002)	July 2001
974	Lian, L., and N. R. Sottos	Stress effects in ferroelectric thin films—*Journal of the Mechanics and Physics of Solids* (submitted)	Aug. 2001
975	Fried, E., and R. E. Todres	Prediction of disclinations in nematic elastomers—*Proceedings of the National Academy of Sciences* **98**, 14773–14777 (2001)	Aug. 2001
976	Fried, E., and V. A. Korchagin	Striping of nematic elastomers—*International Journal of Solids and Structures* **39**, 3451–3467 (2002)	Aug. 2001
977	Riahi, D. N.	On nonlinear convection in mushy layers: Part I. Oscillatory modes of convection—*Journal of Fluid Mechanics* **467**, 331–359 (2002)	Sept. 2001
978	Sofronis, P., I. M. Robertson, Y. Liang, D. F. Teter, and N. Aravas	Recent advances in the study of hydrogen embrittlement at the University of Illinois—Invited paper, Hydrogen–Corrosion Deformation Interactions (Sept. 16–21, 2001, Jackson Lake Lodge, Wyo.)	Sept. 2001
979	Fried, E., M. E. Gurtin, and K. Hutter	A void-based description of compaction and segregation in flowing granular materials—*Continuum Mechanics and Thermodynamics*, in press (2003)	Sept. 2001
980	Adrian, R. J., S. Balachandar, and Z.-C. Liu	Spanwise growth of vortex structure in wall turbulence—*Korean Society of Mechanical Engineers International Journal* **15**, 1741–1749 (2001)	Sept. 2001
981	Adrian, R. J.	Information and the study of turbulence and complex flow—*Japanese Society of Mechanical Engineers Journal B*, in press (2002)	Oct. 2001
982	Adrian, R. J., and Z.-C. Liu	Observation of vortex packets in direct numerical simulation of fully turbulent channel flow—*Journal of Visualization*, in press (2002)	Oct. 2001
983	Fried, E., and R. E. Todres	Disclinated states in nematic elastomers—*Journal of the Mechanics and Physics of Solids* **50**, 2691–2716 (2002)	Oct. 2001
984	Stewart, D. S.	Towards the miniaturization of explosive technology—Proceedings of the 23rd International Conference on Shock Waves (2001)	Oct. 2001
985	Kasimov, A. R., and Stewart, D. S.	Spinning instability of gaseous detonations—*Journal of Fluid Mechanics* (submitted)	Oct. 2001
986	Brown, E. N., N. R. Sottos, and S. R. White	Fracture testing of a self-healing polymer composite—*Experimental Mechanics* (submitted)	Nov. 2001
987	Phillips, W. R. C.	Langmuir circulations—*Surface Waves* (J. C. R. Hunt and S. Sajjadi, eds.), in press (2002)	Nov. 2001
988	Gioia, G., and F. A. Bombardelli	Scaling and similarity in rough channel flows—*Physical Review Letters* **88**, 014501 (2002)	Nov. 2001

List of Recent TAM Reports (cont'd)

No.	*Authors*	*Title*	*Date*
989	Riahi, D. N.	On stationary and oscillatory modes of flow instabilities in a rotating porous layer during alloy solidification—*Journal of Porous Media* **6**, 1–11 (2003)	Nov. 2001
990	Okhuysen, B. S., and D. N. Riahi	Effect of Coriolis force on instabilities of liquid and mushy regions during alloy solidification—*Physics of Fluids* (submitted)	Dec. 2001
991	Christensen, K. T., and R. J. Adrian	Measurement of instantaneous Eulerian acceleration fields by particle-image accelerometry: Method and accuracy—*Experimental Fluids* (submitted)	Dec. 2001
992	Liu, M., and K. J. Hsia	Interfacial cracks between piezoelectric and elastic materials under in-plane electric loading—*Journal of the Mechanics and Physics of Solids* **51**, 921–944 (2003)	Dec. 2001
993	Panat, R. P., S. Zhang, and K. J. Hsia	Bond coat surface rumpling in thermal barrier coatings—*Acta Materialia* **51**, 239–249 (2003)	Jan. 2002
994	Aref, H.	A transformation of the point vortex equations—*Physics of Fluids* **14**, 2395–2401 (2002)	Jan. 2002
995	Saif, M. T. A, S. Zhang, A. Haque, and K. J. Hsia	Effect of native Al_2O_3 on the elastic response of nanoscale aluminum films—*Acta Materialia* **50**, 2779–2786 (2002)	Jan. 2002
996	Fried, E., and M. E. Gurtin	A nonequilibrium theory of epitaxial growth that accounts for surface stress and surface diffusion—*Journal of the Mechanics and Physics of Solids* **51**, 487–517 (2003)	Jan. 2002
997	Aref, H.	The development of chaotic advection—*Physics of Fluids* **14**, 1315–1325 (2002); see also *Virtual Journal of Nanoscale Science and Technology*, 11 March 2002	Jan. 2002
998	Christensen, K. T., and R. J. Adrian	The velocity and acceleration signatures of small-scale vortices in turbulent channel flow—*Journal of Turbulence*, in press (2002)	Jan. 2002
999	Riahi, D. N.	Flow instabilities in a horizontal dendrite layer rotating about an inclined axis—*Journal of Porous Media*, in press (2003)	Feb. 2002
1000	Kessler, M. R., and S. R. White	Cure kinetics of ring-opening metathesis polymerization of dicyclopentadiene—*Journal of Polymer Science A* **40**, 2373–2383 (2002)	Feb. 2002
1001	Dolbow, J. E., E. Fried, and A. Q. Shen	Point defects in nematic gels: The case for hedgehogs—*Proceedings of the National Academy of Sciences* (submitted)	Feb. 2002
1002	Riahi, D. N.	Nonlinear steady convection in rotating mushy layers—*Journal of Fluid Mechanics* **485**, 279–306 (2003)	Mar. 2002
1003	Carlson, D. E., E. Fried, and S. Sellers	The totality of soft-states in a neo-classical nematic elastomer—*Journal of Elasticity* **69**, 169–180 (2003) with revised title	Mar. 2002
1004	Fried, E., and R. E. Todres	Normal-stress differences and the detection of disclinations in nematic elastomers—*Journal of Polymer Science B: Polymer Physics* **40**, 2098–2106 (2002)	June 2002
1005	Fried, E., and B. C. Roy	Gravity-induced segregation of cohesionless granular mixtures—*Lecture Notes in Mechanics*, in press (2002)	July 2002
1006	Tomkins, C. D., and R. J. Adrian	Spanwise structure and scale growth in turbulent boundary layers—*Journal of Fluid Mechanics* (submitted)	Aug. 2002
1007	Riahi, D. N.	On nonlinear convection in mushy layers: Part 2. Mixed oscillatory and stationary modes of convection—*Journal of Fluid Mechanics*, in press (2004)	Sept. 2002
1008	Aref, H., P. K. Newton, M. A. Stremler, T. Tokieda, and D. L. Vainchtein	Vortex crystals—*Advances in Applied Mathematics* **39**, in press (2002)	Oct. 2002
1009	Bagchi, P., and S. Balachandar	Effect of turbulence on the drag and lift of a particle—*Physics of Fluids*, in press (2003)	Oct. 2002
1010	Zhang, S., R. Panat, and K. J. Hsia	Influence of surface morphology on the adhesive strength of aluminum/epoxy interfaces—*Journal of Adhesion Science and Technology* **17**, 1685–1711 (2003)	Oct. 2002

List of Recent TAM Reports (cont'd)

No.	*Authors*	*Title*	*Date*
1011	Carlson, D. E., E. Fried, and D. A. Tortorelli	On internal constraints in continuum mechanics—*Journal of Elasticity* **70**, 101–109 (2003)	Oct. 2002
1012	Boyland, P. L., M. A. Stremler, and H. Aref	Topological fluid mechanics of point vortex motions—*Physica D* **175**, 69–95 (2002)	Oct. 2002
1013	Bhattacharjee, P., and D. N. Riahi	Computational studies of the effect of rotation on convection during protein crystallization—*International Journal of Mathematical Sciences*, in press (2004)	Feb. 2003
1014	Brown, E. N., M. R. Kessler, N. R. Sottos, and S. R. White	*In situ* poly(urea-formaldehyde) microencapsulation of dicyclopentadiene—*Journal of Microencapsulation* (submitted)	Feb. 2003
1015	Brown, E. N., S. R. White, and N. R. Sottos	Microcapsule induced toughening in a self-healing polymer composite—*Journal of Materials Science* (submitted)	Feb. 2003
1016	Kuznetsov, I. R., and D. S. Stewart	Burning rate of energetic materials with thermal expansion—*Combustion and Flame* (submitted)	Mar. 2003
1017	Dolbow, J., E. Fried, and H. Ji	Chemically induced swelling of hydrogels—*Journal of the Mechanics and Physics of Solids*, in press (2003)	Mar. 2003
1018	Costello, G. A.	Mechanics of wire rope—Mordica Lecture, Interwire 2003, Wire Association International, Atlanta, Georgia, May 12, 2003	Mar. 2003
1019	Wang, J., N. R. Sottos, and R. L. Weaver	Thin film adhesion measurement by laser induced stress waves—*Journal of the Mechanics and Physics of Solids* (submitted)	Apr. 2003
1020	Bhattacharjee, P., and D. N. Riahi	Effect of rotation on surface tension driven flow during protein crystallization—*Microgravity Science and Technology* **14**, 36–44 (2003)	Apr. 2003
1021	Fried, E.	The configurational and standard force balances are not always statements of a single law—*Proceedings of the Royal Society* (submitted)	Apr. 2003
1022	Panat, R. P., and K. J. Hsia	Experimental investigation of the bond coat rumpling instability under isothermal and cyclic thermal histories in thermal barrier systems—*Proceedings of the Royal Society of London A* **460**, 1957–1979 (2003)	May 2003
1023	Fried, E., and M. E. Gurtin	A unified treatment of evolving interfaces accounting for small deformations and atomic transport: grain-boundaries, phase transitions, epitaxy—*Advances in Applied Mechanics*, in press (2003)	May 2003
1024	Dong, F., D. N. Riahi, and A. T. Hsui	On similarity waves in compacting media—*Horizons in Physics*, in press (2003)	May 2003
1025	Liu, M., and K. J. Hsia	Locking of electric field induced non-180° domain switching and phase transition in ferroelectric materials upon cyclic electric fatigue—*Applied Physics Letters* **83**, 3978–3980 (2003)	May 2003
1026	Liu, M., K. J. Hsia, and M. Sardela Jr.	In situ X-ray diffraction study of electric field induced domain switching and phase transition in PZT-5H—*Journal of the American Ceramics Society* (submitted)	May 2003
1027	Riahi, D. N.	On flow of binary alloys during crystal growth—*Recent Research Development in Crystal Growth*, in press (2003)	May 2003
1028	Riahi, D. N.	On fluid dynamics during crystallization—*Recent Research Development in Fluid Dynamics*, in press (2003)	July 2003
1029	Fried, E., V. Korchagin, and R. E. Todres	Biaxial disclinated states in nematic elastomers—*Journal of Chemical Physics* **119**, 13170–13179 (2003)	July 2003
1030	Sharp, K. V., and R. J. Adrian	Transition from laminar to turbulent flow in liquid filled microtubes—*Physics of Fluids* (submitted)	July 2003
1031	Yoon, H. S., D. F. Hill, S. Balachandar, R. J. Adrian, and M. Y. Ha	Reynolds number scaling of flow in a Rushton turbine stirred tank: Part I—Mean flow, circular jet and tip vortex scaling—*Chemical Engineering Science* (submitted)	Aug. 2003

List of Recent TAM Reports (cont'd)

No.	*Authors*	*Title*	*Date*
1032	Raju, R., S. Balachandar, D. F. Hill, and R. J. Adrian	Reynolds number scaling of flow in a Rushton turbine stirred tank: Part II—Eigen-decomposition of fluctuation—*Chemical Engineering Science* (submitted)	Aug. 2003
1033	Hill, K. M., G. Gioia, and V. V. Tota	Structure and kinematics in dense free-surface granular flow—*Physical Review Letters*, in press (2003)	Aug. 2003
1034	Fried, E., and S. Sellers	Free-energy density functions for nematic elastomers—*Journal of the Mechanics and Physics of Solids* **52**, 1671–1689 (2004)	Sept. 2003
1035	Kasimov, A. R., and D. S. Stewart	On the dynamics of self-sustained one-dimensional detonations: A numerical study in the shock-attached frame—*Physics of Fluids* (submitted)	Nov. 2003
1036	Fried, E., and B. C. Roy	Disclinations in a homogeneously deformed nematic elastomer—*Nature Materials* (submitted)	Nov. 2003
1037	Fried, E., and M. E. Gurtin	The unifying nature of the configurational force balance—*Mechanics of Material Forces* (P. Steinmann and G. A. Maugin, eds.), in press (2003)	Dec. 2003
1038	Panat, R., K. J. Hsia, and J. W. Oldham	Rumpling instability in thermal barrier systems under isothermal conditions in vacuum—*Philosophical Magazine*, in press (2004)	Dec. 2003
1039	Cermelli, P., E. Fried, and M. E. Gurtin	Sharp-interface nematic–isotropic phase transitions without flow—*Archive for Rational Mechanics and Analysis* (submitted)	Dec. 2003
1040	Yoo, S., and D. S. Stewart	A hybrid level-set method in two and three dimensions for modeling detonation and combustion problems in complex geometries—*Combustion Theory and Modeling* (submitted)	Feb. 2004
1041	Dienberg, C. E., S. E. Ott-Monsivais, J. L. Ranchero, A. A. Rzeszutko, and C. L. Winter	Proceedings of the Fifth Annual Research Conference in Mechanics (April 2003), TAM Department, UIUC (E. N. Brown, ed.)	Feb. 2004
1042	Kasimov, A. R., and D. S. Stewart	Asymptotic theory of ignition and failure of self-sustained detonations—*Journal of Fluid Mechanics* (submitted)	Feb. 2004
1043	Kasimov, A. R., and D. S. Stewart	Theory of direct initiation of gaseous detonations and comparison with experiment—*Proceedings of the Combustion Institute* (submitted)	Mar. 2004
1044	Panat, R., K. J. Hsia, and D. G. Cahill	Evolution of surface waviness in thin films via volume and surface diffusion—*Journal of Applied Physics* (submitted)	Mar. 2004
1045	Riahi, D. N.	Steady and oscillatory flow in a mushy layer—*Current Topics in Crystal Growth Research*, in press (2004)	Mar. 2004
1046	Riahi, D. N.	Modeling flows in protein crystal growth—*Current Topics in Crystal Growth Research*, in press (2004)	Mar. 2004
1047	Bagchi, P., and S. Balachandar	Response of the wake of an isolated particle to isotropic turbulent cross-flow—*Journal of Fluid Mechanics* (submitted)	Mar. 2004
1048	Brown, E. N., S. R. White, and N. R. Sottos	Fatigue crack propagation in microcapsule toughened epoxy—*Journal of Materials Science* (submitted)	Apr. 2004
1049	Zeng, L., S. Balachandar, and P. Fischer	Wall-induced forces on a rigid sphere at finite Reynolds number—*Journal of Fluid Mechanics* (submitted)	May 2004
1050	Dolbow, J., E. Fried, and H. Ji	A numerical strategy for investigating the kinetic response of stimulus-responsive hydrogels—*Journal of the Mechanics and Physics of Solids* (submitted)	June 2004
1051	Riahi, D. N.	Effect of permeability on steady flow in a dendrite layer—*Journal of Porous Media* (submitted)	July 2004